BIOCHEMISTRY

Accelerated Publications

Active State-like Conformational Elements in the β_2-AR and a Photoactivated Intermediate of Rhodopsin Identified by Dynamic Properties of GPCRs[†]

Daniel S. Han, Simon X. Wang, and Harel Weinstein*

Department of Physiology and Biophysics, Weill Medical College, Cornell University, 1300 York Avenue, New York, New York 10021

Received March 14, 2008; Revised Manuscript Received April 30, 2008

ABSTRACT: G-Protein-coupled receptors (GPCRs) adopt various functionally relevant conformational states in cell signaling processes. Recently determined crystal structures of rhodopsin and the β_2-adrenergic receptor (β_2-AR) offer insight into previously uncharacterized active conformations, but the molecular states of these GPCRs are likely to contain both inactive and active-like conformational elements. We have identified conformational rearrangements in the dynamics of the TM7$-$HX8 segment that relate to the properties of the conserved NPxxY(x)5,6F motif and show that they can be used to identify active state-like conformational elements in the corresponding regions of the new structures of rhodopsin and the β_2-AR.

G-Protein-coupled receptors (GPCRs) are integral membrane proteins that share a seven-transmembrane (7-TM) helix bundle architecture observed first for rhodopsin ([1–4]) and more recently for the β_2-adrenergic receptor (β_2-AR) ([5–7]). GPCRs respond to a diverse set of stimuli by switching between conformational states, which enables coupling to specific G-proteins as well as other intracellular binding partners ([8–12]). There is evidence that most elements in the spatially ordered series of conformational changes underlying signal propagation within the TM domain are conserved among rhodopsin-like GPCRs ([8]).

Experimental exploration of structural rearrangements associated with activation have identified point mutations that overcame constraints within the inactive forms and caused constitutive activation ([13–15]). This led to the hypothesis that some of the specific, constraining, interhelical interactions within the TM domain that can be identified in the crystal structures ([1–7]) represent elements of the activation pathway ([8]). The required conformational rearrangements have been shown to take advantage of another feature considered to be conserved across the GPCR family, namely, that the TM helices can incorporate structural perturbations such as bends and kinks, induced by prolines or glycine pairs, where protein flexibility and hinge motions are enabled ([16]).

Together, such considerations led to the concept of identifiable structural motifs (SMs) that are conserved across the GPCR family and take on the role of functional microdomains (FMs) ([8, 9]) working as modular units capable of triggering changes in GPCR conformation and operating as activation switches ([17, 18]). Therefore, a useful framework for describing GPCR conformations associated with function within a given receptor state can involve the systematic assignment of a specific "state" to each FM.

Here we show that such a framework can be useful in characterizing the functional phenotype of a particular GPCR structure, such as in a crystal. For example, the recently

determined crystal structure of rhodopsin (*4*) is thought to be in some intermediate signaling state, and it would therefore not be surprising to find a set of elements, i.e., specific SMs and FMs, that are in an active-like state, whereas others are inactive-like. Similarly, the molecular state of the engineered β_2-AR is ambiguous (*5–7*). This is best illustrated by the finding that the TM3–TM6 salt bridge is broken, a hallmark of activated GPCRs (*7*), yet the protein is crystallized with an inverse agonist that prefers the inactive state so that other regions of the protein may resemble the inactive state represented by the original rhodopsin structure (*1–4*). In both cases, it should be useful to identify those elements that belong to the activated phenotype, which is the cumulative result of a superposition of active-like components related to multiple SMs and FMs. Therefore, we may find that the static crystal structures exhibit some such components, but not others.

We illustrate this novel procedure for the SM/FM comprised of TM7 and the juxtamembrane helix 8 (HX8) that incorporates the widely conserved NPxxY(x)5,6F sequence motif and has been shown to modulate GPCR activation, phosphorylation, and internalization (*19–22*). Biophysical experiments have demonstrated that both TM7 (*23*) and HX8 (*24*), which are seen in all of the GPCR crystals (*1–7*), undergo conformational changes upon receptor activation, suggesting that this SM/FM operates as an activation switch utilized by many rhodopsin-like GPCRs.

In the inactive structure of rhodopsin, the side chains of Y7.53 and F7.60 are close to each other (*1–4*), suggesting a direct interaction. Mutations thought to disrupt this aromatic–aromatic interaction, such as F7.60A, allowed formation of an activated state of rhodopsin, Meta II, but without an accompanying enhancement in G-protein activation (*21*). In the rhodopsin-like serotonin 5-HT2C receptor, Asn substitution of Y7.53 was shown to yield a "locked-on" phenotype in which the receptor has a maximal level of basal signaling that is not reduced by an inverse agonist (*19*). Conversely, mutation of Y7.53 to Phe in this GPCR leads to a "locked-off" phenotype in which the level of basal signaling is completely reduced and cannot be increased by an agonist. Interestingly, the locked-off phenotype can be rescued by a simultaneous Ala substitution at position 7.60. These experiments highlight the interdependence of residues at positions 7.53 and 7.60 in modulating the transition to the active state. Given the high level of structural similarity in this region observed for the β_2-AR (*5–7*) and rhodopsin (*1–4*) and expected from the sequence identities, we speculate that phenotype altering mutations within this SM/FM will produce similar effects in many rhodopsin-like GPCRs, as shown for other components of the activation pathway (*8, 11*).

Because a molecular description of the activation switch involving these residues in GPCR function is still missing, we used molecular dynamics simulations of wild-type (WT) and mutant constructs (see Table 1) of rhodopsin embedded in explicit models of hydrated lipid membranes to provide mechanistic insight into how residues at positions 7.53 and 7.60 modulate receptor dynamics. With regard to the experimentally determined phenotype altering mutations at positions 7.53 and 7.60 of the rhodopsin-like 5-HT2C GPCR (*19*), we studied the dynamic behavior of corresponding rhodopsin mutants (Y7.53N, Y7.53F, F7.60A, Y7.53F/F7.60A, and Y7.53N/F7.60A) with essential dynamics and

Table 1: Systems Studied with Molecular Dynamics Simulation and Phenotypes Characterized Experimentally in 5-HT2C Receptors To enhance robustness and verify reproducibility of the findings, the simulations of the Y7.53F, F7.60A, Y7.53F/F7.60A,and Y7.53N constructs of rhodopsin were repeated in triplicate by starting from the same initial coordinates as the original simulations (26) but with different initial random velocities

	simulation time (ns)	expected phenotype
wild type	45	wild type
F7.60A	12,10,10	slightly reduced activity
Y7.53F	20,14,14	"locked-off"
Y7.53F/F7.60A	12,10,10	similar to wild type
Y7.53N	20,14,14	"locked-on"
Y7.53N/F7.60A	12	unknown

energy calculations to identify molecular indicators of their functional phenotypes. An experimentally unexplored Y7.53N/F7.60A construct was added to the study to investigate how the locked-on phenotype of Y7.53N might be modified by the F7.60A mutation that had rescued the inactive Y7.53F mutant.

We first examined the conformations explored by the cytoplasmic end of TM7 and HX8 [from P303 (7.50) to C323 (7.70)], a segment termed TM7–HX8, using essential dynamics (ED) analysis. ED analysis of structures from the WT simulation (0–20 ns) produced eigenvectors describing the directions of correlated motion. The fraction of the total fluctuation during this initial time interval contributed by the eigenvector that had the highest corresponding eigenvalue describes up to 33% of the overall fluctuations for TM7–HX8, at least twice as much as any other eigenvector. The same analysis was conducted on structures taken from the last 20 ns of the simulation (25–45 ns) and compared with the eigenvectors derived from the 0–20 ns segment. A calculated inner product value of 0.91 indicated that the fluctuations described by the first eigenvector persist throughout the simulation, in contrast to motion described by other eigenvectors. Consequently, the first eigenvector was chosen as a reference vector in the conformational space against which the sampling from the simulations of the mutant constructs can be measured. The average structure of rhodopsin from the WT simulation (0–20 ns) is shown in Figure 1A with arrows assigned to each of the Cα atoms of the TM7–HX8 segment pointing in the positive direction of the reference eigenvector.

The degree of sampling of the reference conformational space was measured by projecting the structures from each simulation onto the first eigenvector derived from the WT simulation. To quantify these findings, the projections were binned and plotted to represent a "projection profile" for each construct. Figure 1C shows that the projection profiles of the WT and the F7.60A construct are both centered around zero, with 47.1 and 44.3% of the conformations, respectively, having projections with negative values. The projection profile of the Y7.53F mutant is dramatically different from that of the WT with 77.2% of the conformations in the negative direction. Notably, the Y7.53F/F7.60A construct, which rescues the locked-off Y7.53F back to the WT-like phenotype in the 5HT-2C receptor (*19*), has projections that favor the positive direction, in the opposite direction from Y7.53F. In contrast, the projection profiles from the simulations of both the Y7.53N and Y7.53N/F7.60A constructs are shifted rightward, to positive values (only 39.8 and 14.7%,
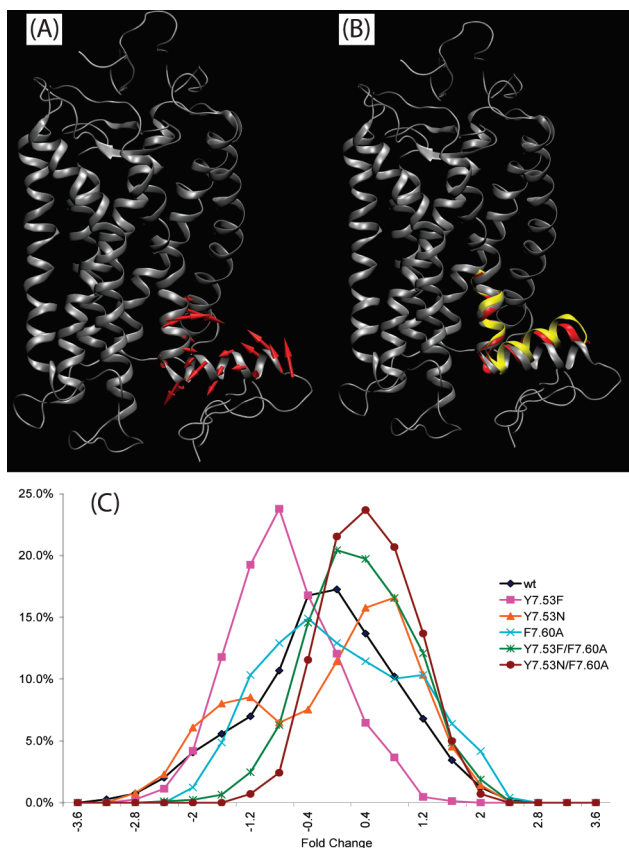
FIGURE 1: (A) Average structure of rhodopsin from the WT simulation (0−20 ns) with arrows indicating the positive direction of motion proportional to the mean square fluctuation of each Cα atom along the reference eigenvector (the first principal eigenvector derived from the WT simulation) for the TM7−HX8 segment. (B) TM7−HX8 segments from the photoactivated rhodopsin intermediate (yellow) and the β_2-AR (red) fitted onto the average structure of inactive rhodopsin from the WT simulation (0−20 ns). Cα atoms for the sequence from position 7.50 to 7.57, and from position 2.40 to 2.43, were used to fit the structures onto each other. Note that these segments lie along the positive direction of the reference eigenvector. (C) Projections of the TM7–HX8 segment from each simulation onto the reference eigenvector, which is the first principal eigenvector derived from the WT simulation. The projections were measured and binned starting from $t = 5$ ns and represent the total distribution from all corresponding trajectories for each construct of rhodopsin (see Table 1). These distributions are plotted as the fold change relative to the mean square fluctuation of the WT simulation along the reference eigenvector.

respectively, are in the negative direction). Clearly, this comparative analysis identifies a metric capable of distinguishing the locked-on Y7.53N from the locked-off Y7.53F and suggests that conformations along this eigenvector may reflect phenotypically important changes in rhodopsin-like GPCRs.

Using this metric, we examined the corresponding TM7−HX8 segments within the most recently determined GPCR crystal structures. The conformations of the TM7−HX8 segments from the photoactivated intermediate of rhodopsin (4) were projected onto the eigenvector derived from the WT simulation, in the same manner that was used for the simulations of the mutant constructs. The projections for the two available chains, B and C (chain A had unresolved residues within this region), were both found to be 2.8-fold greater than the mean square fluctuation seen in the WT trajectory along this eigenvector. These values are in the same

direction as the one favored in the simulation of the Y7.53N construct, which corresponds to the activated (locked-on) form of 5-HT2C (*19*). The structure of the photoactivated intermediate thus exhibits dynamic properties more similar to those of the Y7.53N construct than those of the Y7.53F construct (which in 5-HT2C was shown to be locked-off). A direct comparison with the corresponding segment from the β_2-AR structure (*5–7*) is complicated by the fact that the linker between TM7 and HX8 is one residue shorter in the β_2-AR, but the structural comparison with Figure 1B shows that the TM7−HX8 segment of the β_2-AR lies along the same positive direction of the eigenvector we defined, similar to the locked-on Y7.53N construct and the photoactivated intermediate of rhodopsin (*4*). Therefore, we conclude that the TM7−HX8 segments in both of these GPCR crystal structures resemble active-like conformational elements.

To reveal the intramolecular interactions that underlie the specific dynamic behaviors identified for the TM7−HX8 segments in the various constructs, we calculated interaction energies for the cytoplasmic half of TM7 with adjacent helices, including TM1, TM2, TM6, and HX8 from all simulations. The energies of interaction between TM7 and TM1 were nearly the same for all of the constructs (data not shown), with a standard deviation of only 5.2 kJ/mol calculated from the averages of all of the constructs. The same holds for the energies of interaction between TM7 and TM6 with a standard deviation of 4.8 kJ/mol from the averages of all of the constructs. This is not so for the energy of interaction between TM7 and either TM2 or HX8, with a total standard deviation of 16.8 or 12.6 kJ/mol, respectively, and we are thus able to discriminate the states and conditions.

Surprisingly, it is not the TM7−HX8 interaction energy (Figure 2A) that correlates best with the expected phenotypes of the mutants (Table 1). This interaction energy remains virtually identical in the WT and in the mutants that exhibited the most dramatic phenotypes, locked-on Y7.53N and locked-off Y7.53F. Only the F7.60A substitution, which had little effect on the phenotype in 5-HT2C, significantly diminishes the energy of interaction between TM7 and HX8 (Figure 2A). The specific residue−residue interactions between positions 7.53 and 7.60 are consistent with these findings and show that the F7.60A mutation, but not Y7.53F or Y7.53N, leads to a significant loss of interaction energy relative to that of the WT (Figure 2B), accounting for the majority of the change in the energy of interaction between TM7 and HX8. This argues against the possibility that the mutations at positions Y7.53 and F7.60, which lead to changes in rhodopsin conformation, do so by disrupting the interaction between the two residues (*21*). Interactions among other residues in this local environment are likely associated with the phenotypes observed in 5-HT2C (*19*).

One such set of interactions affected by the mutations at positions 7.53 and 7.60 is between TM7 and TM2 (Figure 2C). While all mutations of Y7.53 lead to a decrease in the energy of interaction between these two regions, due to disrupted 7.53 and N2.40 interactions (Figure 2D), in the locked-on Y7.53N construct the interaction between 7.53 and L2.43 is also weakened (Figure 2E), which results in a total loss of 43 kJ/mol, i.e., 58% lower than WT. In contrast, the TM7−TM2 interaction energy in both locked-off Y7.53F and F7.60A is much less disrupted, being reduced by only 23 kJ/mol (31%) and 9 kJ/mol (12%), respectively, while
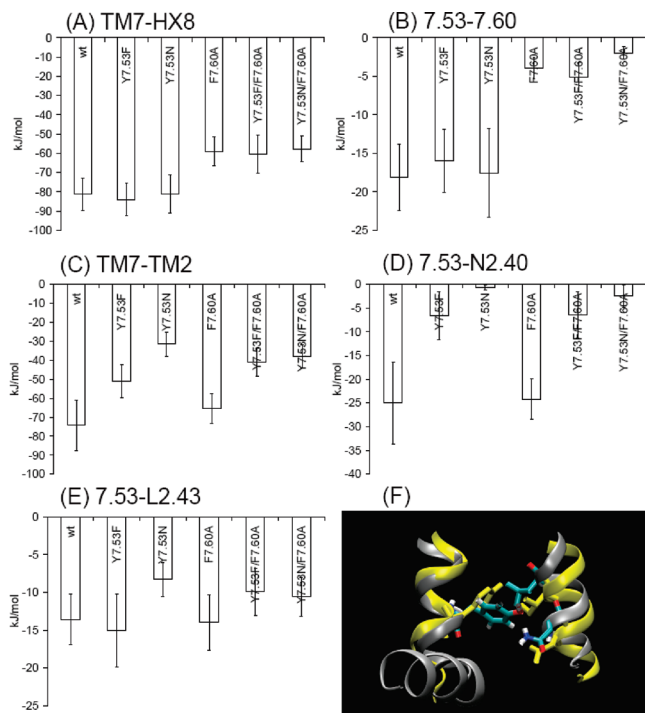
FIGURE 2: Energies of interaction between portions of rhodopsin averaged over the course of the simulation. For the simulations performed in triplicate (Y7.53F, Y7.53N, F7.60A, and Y7.53F/F7.60A), the results represent averages over all of the relevant simulations. The interaction energies were calculated between the following sets of residues: (A) TM7 (7.49−7.56) and HX8 (7.60−7.70), (B) residues at positions 7.53 and 7.60, (C) TM7 (7.49−7.56) and TM2 (2.40−2.50), (D) residues at positions 7.53 and N2.40, and (E) residues at positions 7.53 and L2.43. (F) The color panel shows a representative snapshot of the cytoplasmic ends of TM7 and TM2 from the WT simulation compared to the same region in the β_2-AR structure (yellow). The relative positions of residues Y7.53, N2.40, and L2.43 (I in the β_2-AR) in the two structures suggest a weakened interaction in the β_2-AR structure. Cα atoms corresponding to positions 7.50−7.57 and 2.40−2.43 were used to fit the structures onto each other.

Y7.53F/F7.60A has an intermediate loss of 33 kJ/mol (45%) relative to that of the WT. The magnitude of the TM7−TM2 interaction thus correlates roughly with the expected phenotypes of the 5-HT2C, suggesting that a severe disruption of this interaction beyond a threshold (not reached in the Y7.53F) is a feature of the activation transition. This inference is mechanistically consistent with experiments that found TM2 to be translated away from HX8, and TM7 translated away from TM1 upon photoactivation of rhodopsin (*23, 25*). Therefore, we propose the magnitude of the TM7−TM2 interaction as a property modulated by mutations at positions 7.53 and 7.60 that contributes to the final receptor phenotype, in combination with the TM7−HX8 conformational sampling.

We examined the recently determined GPCR crystal structures in light of our findings concerning the changes in the TM7−TM2 interaction. One noted difference between the β_2-AR crystal structure and that of the inactive rhodopsin crystal structures (*1–3*) is that the aromatic ring of Y7.53 in the β_2-AR is rotated away from HX8 and does not directly interact with residues in TM2 (*5–7, 18*), as seen in Figure 2F. We can now interpret this change, as it is consistent with weakened interactions between TM7 and TM2 observed in the locked-on Y7.53N construct and supports our conclusion

that the conformation of this region of the β_2-AR corresponds to an active-like state. As for the interactions between TM7 and TM2 in the photoactivated intermediate of rhodopsin (*4*), no obvious differences from the inactive models of rhodopsin could be found, leading us to speculate that the disruption in the TM7−TM2 interaction occurs later in the sequence of events along the activation pathway which has not yet been reached by the photoactivated intermediate.

In summary, we used molecular dynamics simulations of mutant constructs of rhodopsin with different activation phenotypes to shed light on the molecular events that are likely to precede and trigger larger structural changes along the GPCR activation path. Two features of GPCR activation regulated by residues 7.53 and 7.60 emerged: the conformation of the TM7−HX8 segment and the energy of interaction between the cytoplasmic ends of TM7 and TM2. Examining these features in the photoactivated deprotonated intermediate structure of rhodopsin, we found support for the proposition that this GPCR structure contains elements of both the activated and inactive receptor phenotypes, as the TM7−HX8 segment resembled an active-like conformation while the TM7−TM2 interaction was still intact, resembling an inactive-like state. Similarly, in the experimentally unexplored construct, Y7.53N/F7.60A (Table 1), the conformational sampling of the TM7−HX8 segment resembled that of locked-on Y7.53N (see Figure 1C), yet the TM7−TM2 interaction energy was only partially disrupted (Figure 2C). Thus, we predict that a Y7.53N/F7.60A 5-HT2C construct would have an intermediate phenotype between Y7.53N and the WT, where the F7.60A mutation acts to mitigate the extreme phenotype of locked-on Y7.53N and brings it closer to WT levels, similar to the F7.60A rescue of locked-off Y7.53F (*19*). Interestingly, in the β_2-AR, both the TM7−HX8 segment and the loss of direct interaction between Y7.53 and TM2 suggest that this region adopts an active-like state, reflected by the β_2-AR−T4 chimera having an enhanced affinity for agonists, but not antagonists (*7*). Given the complex nature of the structural changes in the properties of the SM/FM associated with the active and inactive states, it is not entirely surprising that the crystal structure of the β_2-AR includes some active-like elements. Thus, the receptor has a higher basal activity than rhodopsin; carazolol has a weak inverse agonist potency, and the chimeric additions between TM5 and TM6 may affect the adjacent TM7.

SUPPORTING INFORMATION AVAILABLE

Molecular dynamics simulation details, model construction, essential dynamics analysis, and GPCR numbering system. This material is available free of charge via the Internet at http://pubs.acs.org.

REFERENCES

1. Palczewski, K., Kumasaka, T., Hori, T., Behnke, C. A., Motoshima, H., Fox, B. A., Le Trong, I., Teller, D. C., Okada, T., Stenkamp, R. E., Yamamoto, M., and Miyano, M. (2000) Crystal structure of rhodopsin: A G protein-coupled receptor. *Science 289*, 739–745.
2. Teller, D. C., Okada, T., Behnke, C. A., Palczewski, K., and Stenkamp, R. E. (2001) Advances in determination of a high-resolution three-dimensional structure of rhodopsin, a model of G-protein-coupled receptors (GPCRs). *Biochemistry 40*, 7761–7772.
3. Okada, T., Fujiyoshi, Y., Silow, M., Navarro, J., Landau, E. M., and Shichida, Y. (2002) Functional role of internal water molecules

in rhodopsin revealed by X-ray crystallography. *Proc. Natl. Acad. Sci. U.S.A. 99*, 5982–5987.

4. Salom, D., Lodowski, D. T., Stenkamp, R. E., Le Trong, I., Golczak, M., Jastrzebska, B., Harris, T., Ballesteros, J. A., and Palczewski, K. (2006) Crystal structure of a photoactivated deprotonated intermediate of rhodopsin. *Proc. Natl. Acad. Sci. U.S.A. 103*, 16123–16128.

5. Cherezov, V., Rosenbaum, D. M., Hanson, M. A., Rasmussen, S. G., Thian, F. S., Kobilka, T. S., Choi, H. J., Kuhn, P., Weis, W. I., Kobilka, B. K., and Stevens, R. C. (2007) High-resolution crystal structure of an engineered human β2-adrenergic G protein-coupled receptor. *Science 318*, 1258–1265.

6. Rasmussen, S. G., Choi, H. J., Rosenbaum, D. M., Kobilka, T. S., Thian, F. S., Edwards, P. C., Burghammer, M., Ratnala, V. R., Sanishvili, R., Fischetti, R. F., Schertler, G. F., Weis, W. I., and Kobilka, B. K. (2007) Crystal structure of the human β2 adrenergic G-protein-coupled receptor. *Nature 450*, 383–387.

7. Rosenbaum, D. M., Cherezov, V., Hanson, M. A., Rasmussen, S. G., Thian, F. S., Kobilka, T. S., Choi, H. J., Yao, X. J., Weis, W. I., Stevens, R. C., and Kobilka, B. K. (2007) GPCR engineering yields high-resolution structural insights into β2-adrenergic receptor function. *Science 318*, 1266–1273.

8. Filizola, M., and Weinstein, H. (2005) The structure and dynamics of GPCR oligomers: A new focus in models of cell-signaling mechanisms and drug design. *Curr. Opin. Drug Discovery Dev. 8*, 577–584.

9. Visiers, I., Ballesteros, J. A., and Weinstein, H. (2002) Three-dimensional representations of G protein-coupled receptor structures and mechanisms. *Methods Enzymol. 343*, 329–371.

10. Kristiansen, K. (2004) Molecular mechanisms of ligand binding, signaling, and regulation within the superfamily of G-protein-coupled receptors: Molecular modeling and mutagenesis approaches to receptor structure and function. *Pharmacol. Ther. 103*, 21–80.

11. Kobilka, B. K. (2007) G protein coupled receptor structure and activation. *Biochim. Biophys. Acta 1768*, 794–807.

12. Kobilka, B. K., and Deupi, X. (2007) Conformational complexity of G-protein-coupled receptors. *Trends Pharmacol. Sci. 28*, 397–406.

13. Seifert, R., and Wenzel-Seifert, K. (2002) Constitutive activity of G-protein-coupled receptors: Cause of disease and common property of wild-type receptors. *Naunyn-Schmiedeberg's Arch. Pharmacol. 366*, 381–416.

14. Han, M., Smith, S. O., and Sakmar, T. P. (1998) Constitutive activation of opsin by mutation of methionine 257 on transmembrane helix 6. *Biochemistry 37*, 8253–8261.

15. Kim, J. M., Altenbach, C., Kono, M., Oprian, D. D., Hubbell, W. L., and Khorana, H. G. (2004) Structural origins of constitutive activation in rhodopsin: Role of the K296/E113 salt bridge. *Proc. Natl. Acad. Sci. U.S.A. 101*, 12508–12513.

16. Sansom, M. S., and Weinstein, H. (2000) Hinges, swivels and switches: The role of prolines in signalling via transmembrane α-helices. *Trends Pharmacol. Sci. 21*, 445–451.

17. Smit, M. J., Vischer, H. F., Bakker, R. A., Jongejan, A., Timmerman, H., Pardo, L., and Leurs, R. (2007) Pharmacogenomic and structural analysis of constitutive G protein-coupled receptor activity. *Annu. Rev. Pharmacol. Toxicol. 47*, 53–87.

18. Bhattacharya, S., Hall, S. E., Li, H., and Vaidehi, N. (2007) Ligand Stabilized Conformational States of Human β2 Adrenergic Receptor: Insight into G Protein Coupled Receptor Activation. *Biophys. J.* . (in press).

19. Prioleau, C., Visiers, I., Ebersole, B. J., Weinstein, H., and Sealfon, S. C. (2002) Conserved helix 7 tyrosine acts as a multistate conformational switch in the 5HT2C receptor. Identification of a novel "locked-on" phenotype and double revertant mutations. *J. Biol. Chem. 277*, 36577–36584.

20. Kalatskaya, I., Schussler, S., Blaukat, A., Muller-Esterl, W., Jochum, M., Proud, D., and Faussner, A. (2004) Mutation of tyrosine in the conserved NPXXY sequence leads to constitutive phosphorylation and internalization, but not signaling, of the human B2 bradykinin receptor. *J. Biol. Chem. 279*, 31268–31276.

21. Fritze, O., Filipek, S., Kuksa, V., Palczewski, K., Hofmann, K. P., and Ernst, O. P. (2003) Role of the conserved NPxxY(x)5,6F motif in the rhodopsin ground state and during activation. *Proc. Natl. Acad. Sci. U.S.A. 100*, 2290–2295.

22. Anavi-Goffer, S., Fleischer, D., Hurst, D. P., Lynch, D. L., Barnett-Norris, J., Shi, S., Lewis, D. L., Mukhopadhyay, S., Howlett, A. C., Reggio, P. H., and Abood, M. E. (2007) Helix 8 Leu in the CB1 cannabinoid receptor contributes to selective signal transduction mechanisms. *J. Biol. Chem. 282*, 25100–25113.

23. Altenbach, C., Cai, K., Klein-Seetharaman, J., Khorana, H. G., and Hubbell, W. L. (2001) Structure and function in rhodopsin: Mapping light-dependent changes in distance between residue 65 in helix TM1 and residues in the sequence 306−319 at the cytoplasmic end of helix TM7 and in helix H8. *Biochemistry 40*, 15483–15492.

24. Lehmann, N., Alexiev, U., and Fahmy, K. (2007) Linkage between the intramembrane H-bond network around aspartic acid 83 and the cytosolic environment of helix 8 in photoactivated rhodopsin. *J. Mol. Biol. 366*, 1129–1141.

25. Altenbach, C., Klein-Seetharaman, J., Cai, K., Khorana, H. G., and Hubbell, W. L. (2001) Structure and function in rhodopsin: Mapping light-dependent changes in distance between residue 316 in helix 8 and residues in the sequence 60−75, covering the cytoplasmic end of helices TM1 and TM2 and their connection loop CL1. *Biochemistry 40*, 15493–15500.

26. Filizola, M., Wang, S. X., and Weinstein, H. (2006) Dynamic models of G-protein coupled receptor dimers: Indications of asymmetry in the rhodopsin dimer from molecular dynamics simulations in a POPC bilayer. *J. Comput.-Aided Mol. Des. 20*, 405–416.

27. Delano, W. L. (2002) The PyMOL Molecular Graphics System, DeLano Scientific, San Carlos, CA.

28. Van Der Spoel, D., Lindahl, E., Hess, B., Groenhof, G., Mark, A. E., and Berendsen, H. J. (2005) GROMACS: Fast, flexible, and free. *J. Comput. Chem. 26*, 1701–1718.

29. Amadei, A., Linssen, A. B., and Berendsen, H. J. (1993) Essential dynamics of proteins. *Proteins 17*, 412–425.

30. van Aalten, D. M., Amadei, A., Linssen, A. B., Eijsink, V. G., Vriend, G., and Berendsen, H. J. (1995) The essential dynamics of thermolysin: Confirmation of the hinge-bending motion and comparison of simulations in vacuum and water. *Proteins 22*, 45–54.

31. Faraldo-Gomez, J. D., Forrest, L. R., Baaden, M., Bond, P. J., Domene, C., Patargias, G., Cuthbertson, J., and Sansom, M. S. (2004) Conformational sampling and dynamics of membrane proteins from 10-nanosecond computer simultations. *Proteins. 57*, 783–791.

32. Ballesteros, J., and Weinstein, H. (1995) Integrated methods for the construction of three-dimensional models of structure-function relations in G protein-coupled receptors. *Methods Neurosci. 25*, 366–428.

33. Humphrey, W., Dalke, A., and Schulten, K. (1996) VMD: Visual molecular dynamics. *J. Mol. Graphics 14* (33−38), 27–38.